




Open Archive Toulouse Archive Ouverte (OATAO)

OATAO is an open access repository that collects the work of Toulouse researchers and makes it freely available over the web where possible

This is an author's version published in: <http://oatao.univ-toulouse.fr/8759>

Official URL: <https://doi.org/10.1088/0957-4484/23/50/505206>

To cite this version:

Corde, Jöelle and Perruchas, Sandrine and Vieille, Laetitia and Galaup, Jean-Pierre and Duluard, Sandrine Nathalie  and Biver, Claudine and Boilot, Jean-Pierre and Gacoin, Thierry *Photolithographic processing of silver loaded dielectric coatings based on preformed colloidal TiO₂nanoparticles dispersed in a mesoporous silica binder.* (2012) *Nanotechnology*, 23 (50). 1-9. ISSN 0957-4484

Any correspondence concerning this service should be sent to the repository administrator: tech-oatao@listes-diff.inp-toulouse.fr

Photolithographic processing of silver loaded dielectric coatings based on preformed colloidal TiO₂ nanoparticles dispersed in a mesoporous silica binder

Jöelle Corde¹, Sandrine Perruchas¹, Laetitia Vieille¹,
Jean-Pierre Galaup², Sandrine Duluard³, Claudine Biver³,
Jean-Pierre Boilot¹ and Thierry Gacoin¹

¹ Laboratoire de Physique de la Matière Condensée, Ecole Polytechnique—CNRS, Palaiseau, F-91128, France

² Laboratoire Aimé Cotton, CNRS UPR 3321 & Université Paris 11, Bât. 505, Campus d'Orsay, F-91405, Orsay, France

³ ESSILOR International, Rue Pierre et Marie Curie, F-31682 Labège, France

E-mail: thierry.gacoin@polytechnique.edu

Abstract

Titanium dioxide is a well known photocatalyst for reactions involving surface trapped photogenerated carriers. Noble metal photo-reduction may be used for the processing of silver/TiO₂ nanocomposite coatings that may exhibit interesting optical and electrical properties. We present here results of our investigations performed on an original system consisting of preformed colloidal TiO₂ nanoparticles homogeneously dispersed within a mesoporous silica host matrix. Light irradiation of samples immersed in an aqueous silver salt solution leads to the homogeneous deposition of silver islands in the vicinity of the TiO₂ particles and throughout the film thickness. The silver volume fraction is directly controlled by the irradiation dose up to a value of about 16 vol.%. Films exhibit tunable plasmonic properties that correspond to silver nanoparticles in interaction, and a percolation threshold is observed at 8–10 vol.%, leading to films with a conductivity of about 40 S cm⁻¹. The major interest of this method lies in the high silver reduction quantum efficiency (about 50%) and the possibility to modulate optical and electronic properties by light irradiation while the low temperature of processing permits the photolithographic deposition of metallic patterns on organic flexible substrates.

(Some figures may appear in colour only in the online journal)



1. Introduction

Titanium dioxide is a well known semiconductor compound with remarkable dielectric, electronic and physico-chemical surface properties [1]. This has led to many applications such as solar cells and photocatalysis, the latter being extensively studied for practical applications in decontamination or

self-cleaning devices [2]. The basic principle relies on the high redox activity of photogenerated carriers and radicals resulting from their reaction with adsorbed species at the surface of the oxide. The reduction properties of photogenerated electrons are easily demonstrated by considering the formation of noble metal precipitates through UV irradiation of TiO₂ powders under the presence of the

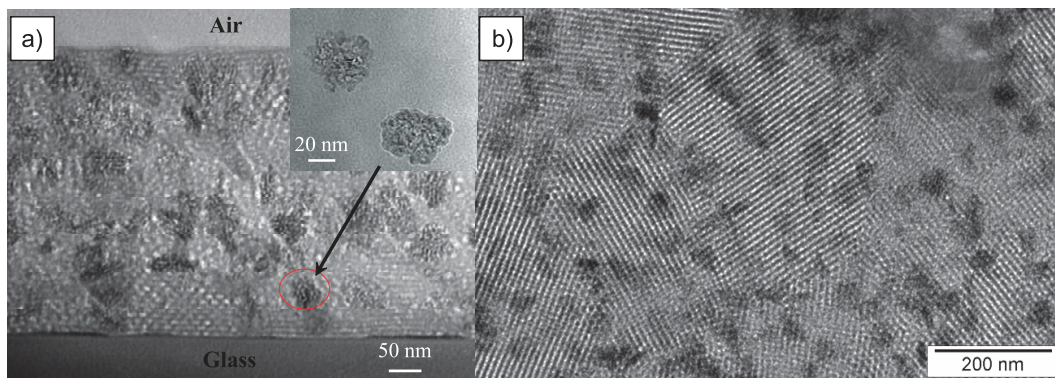


Figure 1. Transmission electron microscopy image of a typical film made using CG-TiO₂ particles. (a) Transverse section view with a TiO₂/SiO₂ molar ratio equal to 0.25. The inset shows the particles before insertion into the film [17]. (b) In plane view with a TiO₂/SiO₂ molar ratio equal to 0.05. White dots in the images correspond to the mesopores, whose size is about 5 nm.

metal salt. This phenomenon has been known for a long time with early applications for silver recovery from photographic wastes [3] and for the development of original photo-imaging processes [4]. It has also been extended to different high bandgap semiconductors such as ZnO [5] or CdSe [6, 7] for the elaboration of colloidal hybrid nanostructures [8].

Photocatalytic photo-reduction has also been applied for the synthesis of metal/dielectric coatings, especially using sol-gel titania coatings. In 2000, Lianos and co-workers reported the photocatalytic deposition of silver particles within mesoporous sol-gel TiO₂ films after adsorption of silver ions [9]. In a series of papers, Tatsuma and co-workers studied optical properties and evidenced some reversibility in the photo-reduction process that relies on the possible back photo-excitation of electrons from the metal islands into the TiO₂ conduction band under visible irradiation. This leads to multicolor photochromism associated with the rearrangement of the silver phase [10–15].

Recently, Soler-illia and co-workers investigated conduction properties of highly loaded silver/TiO₂ films and demonstrated the potentialities of the photo-reduction strategy for the lithographic deposition of patterned metallic electrodes [16]. This work was achieved on mesoporous titania films which were obtained after calcination of a sol-gel formulation including an organic pore templating agent. Thermal treatment allows the removal of the organic species and the crystallization of the precursors into anatase nanocrystallites.

In the present work, this strategy is investigated the case of films that are obtained through the dispersion of preformed colloidal TiO₂ nanoparticles into a mesoporous silica binder (figure 1) [17, 18]. This approach, as compared to others, takes advantage of the mesoporous silica binder to ensure good mechanical properties of the films while keeping a control of the porous microstructure to ensure the chemical accessibility to the TiO₂ particle surface. More interestingly, the use of preformed colloidal particles also allows investigation of different parameters such as the particle size and concentration, also opening the way toward the use of other colloidal formulations such as doped TiO₂ nanoparticles or other semiconductors that can be prepared

as colloidal suspensions. Moreover, the used of preformed particles with an excellent crystallinity do not require any further thermal treatments so that functional coatings on polymer substrates are possible with a view to designing patterned devices on flexible substrates.

The first part of this work details the elaboration process of the films and the photocatalytic silver loading experiment. The second part is devoted to the investigation of the silver particle formation mechanism and the determination of the silver deposition quantum yield. The influence of the film porosity is discussed with respect to the silver distribution within the film thickness and the maximum silver loading. The last part provides detailed characterizations of the physical properties of the films, considering both optical properties (such as plasmonic absorption and photochromism) and conduction properties as a function of the metal loading.

2. Experimental details

2.1. Thin film synthesis

The elaboration of the photocatalytic films was directly adapted from our previous work [17]. In a typical experiment, tetraethoxysilane or TEOS (5.5 ml, Aldrich), absolute ethanol (5.5 ml, Aldrich) and an aqueous acidic solution of HCl pH 1.25 (2.25 ml) are mixed under vigorous stirring. The obtained solution is then heated for 1 h at 60 °C and cooled down to room temperature. To the latter solution is added the copolymer (PE6800, BASF) dissolved in ethanol with a volume twice that of the TEOS solution and with a concentration corresponding to a copolymer/silica molar ratio of 0.01. The colloidal suspension of TiO₂ particles is then added dropwise to this solution. Standard experiments are achieved with a TiO₂/SiO₂ molar ratio equal to 1, but lower ratios (0.05 or 0.025) may be used for TEM characterizations. The resulting solution is deposited on a glass or polyester (PEN: polyethylene naphthalate) substrate by spin-coating with a rotation speed of 2000 rpm. For samples with a bilayer structure, the top porous silica buffer layer is deposited from a sol with the same composition as the previous layer but without the TiO₂ particles. In all cases, after drying in air,

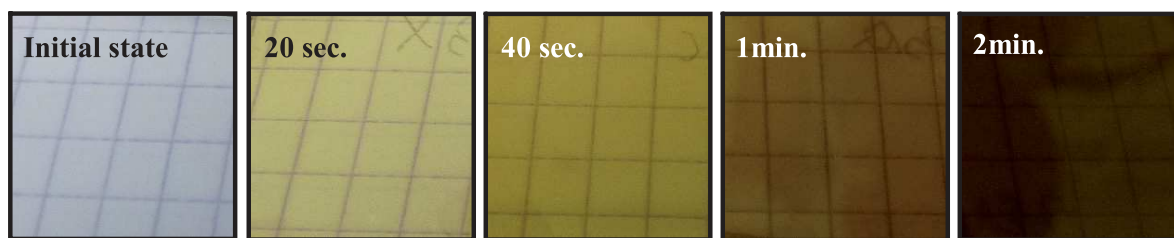


Figure 2. Picture of films (standard composition with $\text{TiO}_2/\text{SiO}_2 = 1$) that have been subjected to different times of irradiation (3.5 mW cm^{-2}) in the presence of Ag^+ ions in solution.

the films may be either thermally treated at 450°C for 2 h to remove the copolymer template (films on glass substrates), or left in an oven at 110°C for 12 h (polymer substrates).

Two types of particles were used but most experiments were achieved using commercial TiO_2 particles (denoted CG- TiO_2) purchased from Cristal Global (reference S5-300 A). The concentration of particles was measured as $C(\text{TiO}_2) = 230 \text{ g l}^{-1}$ using thermogravimetry. For the purpose of our study, some experiments were also carried out using smaller TiO_2 nanoparticles (referred to as S- TiO_2) synthesized in the laboratory by TiCl_4 hydrolysis, following the process adapted from the work of Serpone (see details in supplementary information, available at stacks.iop.org/Nano/23/505206/mmedia) [19]. In this case, the particle size was measured as about 7 nm using dynamic light scattering (Malvern Zetasizer) and the concentration was measured as $C(\text{TiO}_2) = 80 \text{ g l}^{-1}$ using thermogravimetry.

Figure 1 provides TEM pictures of a typical film 450 nm thick on glass substrate synthesized with CG- TiO_2 particles. The TiO_2 particles are homogeneously dispersed within the mesoporous silica matrix. Note that, as shown in the inset of figure 1(a), these particles consist of aggregates with a size of about 50 nm, formed by the assembly of primary particles of about 5 nm. White dots in the TEM image correspond to mesopores with a size of typically 5 nm as templated by the initial copolymer micelles. In addition to the mesopores, previous detailed investigation of the porosity of the films revealed some microporosity resulting from the incomplete condensation of the silica walls between the mesopores [18]. This leads to an interconnection between the pores which makes possible the complete impregnation of the films by chemicals and ensures diffusion pathways toward the surface for the TiO_2 particles.

2.2. Silver photo-reduction experiments

Photo-reduction experiments were simply achieved through immersion of the films in a 0.05 M $\text{AgNO}_3/\text{H}_2\text{O}$ –isopropanol (1:1 volume ratio) solution. The thickness of the solution above the film is about 5 mm. A description of the experimental setup is given in figure 1 of the supplementary information (available at stacks.iop.org/Nano/23/505206/mmedia). After 2 min of immersion, the film in the solution is exposed to 312 nm radiation from a standard 3.5 mW cm^{-2} UV lamp for various durations. Upon irradiation, the initially transparent film develops a yellow color within about 20 s that turns progressively dark brown.

2.3. Characterizations

UV–vis spectra were recorded in the 350–3000 nm range, with a Varian Cary 500 spectrophotometer. Transmission electron microscopy (TEM) experiments were recorded on a 300 keV Philips CM30. Micrographs were processed with a slow scan CCD camera and analyzed with the Digital Micrograph program. Scanning electron microscopy (SEM) analysis: electron microscopy experiments were realized using an FEG-SEM Hitachi 4800 operating between 1 and 10 kV. Film resistivity was determined at room temperature as a function of the silver loading from four-point van der Pauw measurements using a Microworld resistivity stand (S302-x). The given values are the average of five independent experiments performed on different films irradiated for the same time.

3. Results and discussion

3.1. Color evolution upon irradiation

Figure 2 shows the typical evolution of films after increasing times of irradiations. No significant differences were noticed in term of color and kinetics considering films deposited either on glass or on polymer substrates: increasing the irradiation time results in a color change from yellow to dark brown and then almost black.

These colors are characteristic of the formation of silver islands, which exhibit plasmonic resonances [20] with an absorption band around 420 nm (see spectra figure 3(a)). The catalytic effect of the TiO_2 particles was checked by achieving a blank experiment on a film without particles. In that case, no visible absorption was seen after 2 h of irradiation. The effect of isopropanol as a hole scavenger was shown by an increase of the reduction efficiency of 60% as compared to solutions without isopropanol. Similar experiments may be achieved on dried films into which Ag^+ ions have been previously adsorbed by immersion in a silver salt solution before washing and drying. In this case, the yellow color develops, but its intensity saturates after short irradiation times due to the limited number of available silver ions. Further experiments were thus exclusively achieved through irradiation on films directly immersed in the silver salt solution.

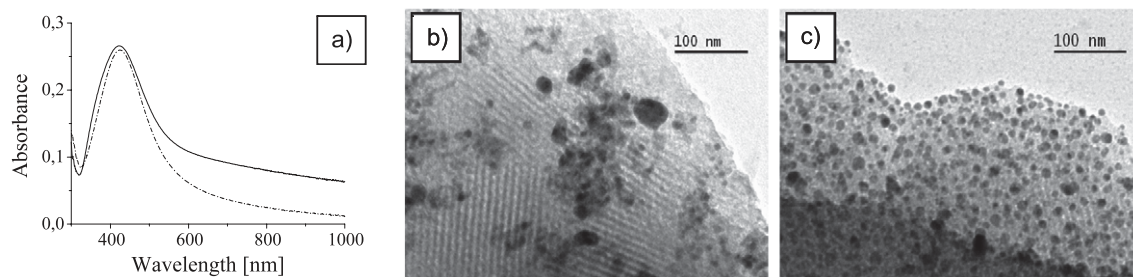


Figure 3. (a) Absorption spectra of films with either 50 nm CG-TiO₂ particles (plain line) or 7 nm S-TiO₂ particles (dotted line). TEM pictures of corresponding films showing the distribution of silver particles: CG-TiO₂ film (b) and S-TiO₂ film (c).

3.2. Characterization of the particles and mechanism of formation

Figure 3 shows a TEM image of typical films prepared with the same volume fraction ($Ti/Si = 0.05$) of 50 nm CG-TiO₂ and 7 nm S-TiO₂ particles respectively, after two different times of irradiation leading to similar silver loadings (about 1%). In both cases, silver particles are clearly visible with a much higher contrast than the TiO₂ particles.

As shown in previous works [21], the mechanism of the Ag particle formation is well explained in terms of reduction of surrounding silver ions by the photogenerated electrons trapped at the surface of the TiO₂ particles. A major difference is seen between the two samples considering the silver particle size and global distribution within the film. This clearly reflects the distribution of the initial TiO₂ particles that were incorporated with the same concentration but strongly differ in size so that the number of particles per unit volume is much more important in the S-TiO₂ sample. This indicates unsurprisingly that the silver particles are formed directly at the TiO₂ surface. Several silver particles are visible around each CG-TiO₂ particle, while the homogeneity of the size distribution indicates that probably one silver particle is formed for each TiO₂ nanocrystal in the S-TiO₂ case. Previous works, recently reviewed by Costi and co-workers, have shown heterogeneous nucleation of metal on specific polar facets of anisotropic semiconductor particles such as nanorods [8]. The polycrystalline nature of the CG-TiO₂ particles (see inset in figure 1(a)) probably explains the nucleation of several silver particles at their surface. Starting from small silver germs, further growth is favored rather than new surface nucleation. This is explained by the transfer of photogenerated electrons through Fermi level equilibration at the Schottky junction [22]. Electrons then tend to be stored on pre-existing silver islands, allowing further reaction with surrounding silver ions. In the case of the CG-TiO₂, we observe a large distribution of silver particle size, which is probably explained by the size distribution of the primary crystallites forming the TiO₂ particles, or more or less favorable exposed surfaces for electron trapping. Considering our specific case of particle growth within a mesoporous silica matrix, it must be noted that the size of the particles is not limited by the size of the silica mesopores (5 nm). This is similar to previous works involving thermal or chemical reduction of silver in mesoporous films, showing that the

silver growth is able to push the porous silica walls to some extent [23].

3.3. Investigation of the kinetics of silver deposition up to high silver loading

Experiments were achieved to investigate the kinetics of silver deposition and to characterize the film properties up to high silver loading. Preliminary studies showed that long irradiation times lead to an inhomogeneous metallic deposit at the surface of the films, corresponding to the growth of very large silver crystals (figure 2(a) supplementary information (available at stacks.iop.org/Nano/23/505206/mmedia)). After some reduction of silver within the film, conductive percolation pathways toward the film/solution interface are formed. Photogenerated electrons within the film are able to diffuse to the interface and react with silver ions directly from the solution, leading to unconfined silver growth at the film surface. Improvement was obtained following the approach of Martinez and co-workers [16], using a porous silica layer 150 nm thick deposited on top of the active TiO₂ loaded film before the photo-reduction experiment. In this case, the silver particles remain confined within the photo-active layer, with no extension at the interface with the solution (figure 4(b)). All further experiments have thus been achieved with this bilayer configuration.

Figure 4(a) presents the typical evolution of the extinction of a CG-TiO₂ film in the 350–3000 nm range for irradiation times up to 2 h. After a first step of initiation, continuous increase of the whole spectrum is observed while its shape is globally preserved over all the wavelength range. Spherical silver nanoparticles are well known to exhibit an intense plasmonic absorption band peaking at about 400–420 nm in media with refractive index of 1.4–1.5. The large extension of the plasmonic extinction toward the infrared in our samples has to be accounted for. It is well known that particles with anisotropic shapes do exhibit significant extinction in the red to infrared region, with a position in energy that depends on the particle morphology. In our case, the large spreading of the extinction could thus be explained by a very large distribution of particle morphologies. Nevertheless, a closer examination of the extinction spectra of our samples at the initial stage of irradiation led us to consider another explanation. Figure 3(a) shows the extinction spectra of CG-TiO₂ and S-TiO₂ samples with low silver loading. We clearly see that the CG-TiO₂

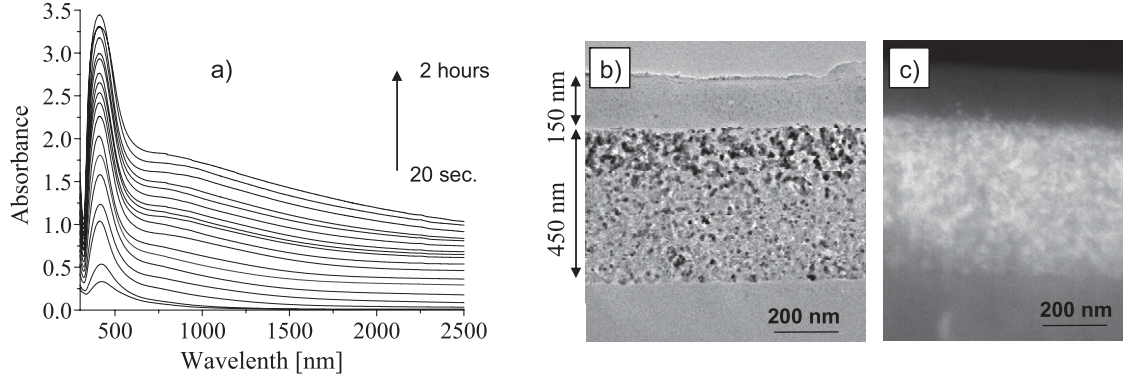


Figure 4. (a) Evolution of the absorption spectra of bilayer films irradiated from 20 s to 2 h (3.5 mW cm^{-2}). (b) TEM cross-section view of a film after 3.5 min of irradiation. (c) SEM cross-section view of a film after 30 min of irradiation.

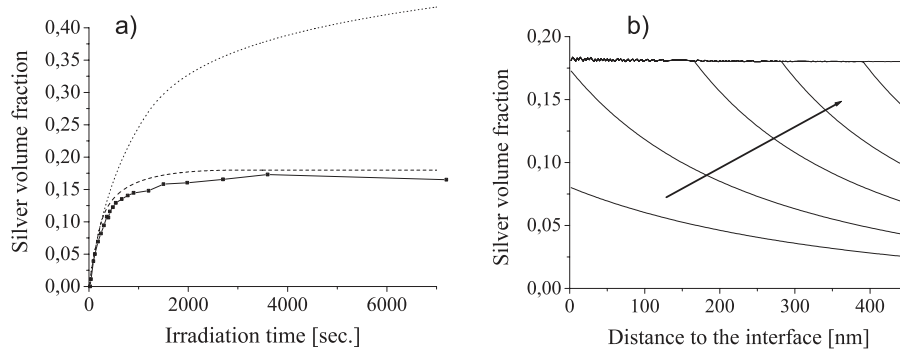


Figure 5. (a) Kinetics of the evolution of the silver loading as a function of the irradiation time. Black dots correspond to experimental points. The dotted line is the result of the calculation assuming a 100% maximum loading. The dashed line is the result of the calculation limiting the loading to a volume fraction of 18%. (b) Calculated evolution of the silver loading profile for increasing irradiation times assuming a maximum possible loading of 18%.

already exhibits a significant contribution in the red/IR, in contrast to what is seen for the S-TiO₂ sample. Considering the difference of the spatial distribution of the silver particles between the two samples, we conclude that, in addition to a distribution of shape anisotropy, at least part of the red/NIR contribution may result from plasmonic interactions between particles. Such interactions occur at lower silver loading in the case of the CG-TiO₂ sample because several silver particles are confined around each TiO₂ particle.

To investigate the kinetics of silver reduction, the silver loading was determined by chemical analysis after different irradiation times. After an induction period of about one minute, a linear relationship is found between the absorbance at different wavelengths and the silver content within the film (figure 3 supplementary information, available at stacks.iop.org/Nano/23/505206/mmedia). Considering that the absorbance A_{Ag} of silver in the film can be expressed as $A_{Ag} = \alpha_{Ag} \rho_{Ag} e / \ln(10)$, where ρ_{Ag} is the silver volume fraction in the film and e the film thickness (in nm), the extinction coefficient α_{Ag} is found to be equal to $1/41 \text{ nm}^{-1}$, $1/11 \text{ nm}^{-1}$ and $1/20 \text{ nm}^{-1}$ at 320, 410 and 1000 nm respectively. These values may be compared to values reported for bulk silver, which are equal to $1/50 \text{ nm}^{-1}$, $1/15 \text{ nm}^{-1}$ and $1/11 \text{ nm}^{-1}$ respectively for the same wavelengths [24].

Figure 5(a) presents the evolution of the silver content (ρ_{Ag}) in the films as a function of the irradiation time (t). At the beginning of the reduction process, the slope of the curve may be expressed as

$$\rho_{Ag}(t=0) = \eta P_0 \frac{V_{Ag}}{N_A e} (1 - 10^{-A_{TiO_2}}) \quad (1)$$

with η the quantum yield of silver reduction, P_0 the power of the UV source (in photons $\text{s}^{-1} \text{ nm}^{-2}$), V_{Ag} the molar volume of silver, N_A the Avogadro constant, e the film thickness and A_{TiO_2} the absorbance of TiO₂ in the film. The number of absorbed photons (corresponding to $P_0(1 - 10^{-A_{TiO_2}})$) can be calculated considering the absorbance of the film, the emission spectrum of the UV lamp, and its global power of emission (3.5 mW cm^{-2}), leading to $P_0 = 29.4 \text{ photons s}^{-1} \text{ nm}^{-2}$ (figure 4 supplementary information, available at stacks.iop.org/Nano/23/505206/mmedia). We thus deduce from the slope at the origin ($5.67 \cdot 10^{-4} \% \text{ Ag s}^{-1}$) that the quantum yield of silver reduction is about 51%. To our knowledge, no data allowing for comparison have yet been reported in the literature. This high value nevertheless evidences the high efficiency of the photo-reduction process as shown by the rapid development of the film coloration upon the irradiation process (figure 2).

The evolution of the curve in figure 5(a) clearly shows saturation for silver loading of about 16%. Considering that

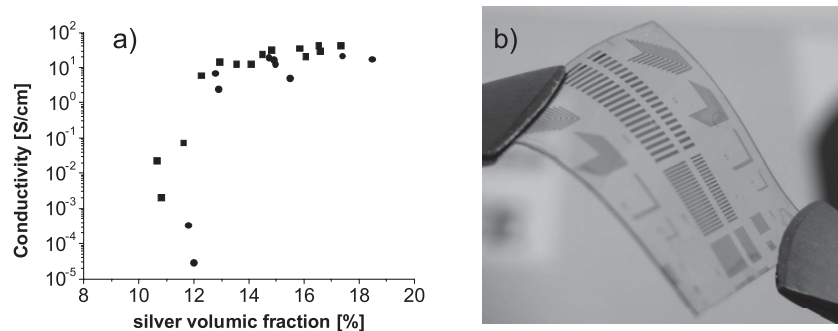


Figure 6. (a) Evolution of the conductivity as a function of the silver loading. Squares and dots correspond to data measured on CG-TiO₂ and S-TiO₂ films respectively. (b) Image of silver patterns formed on a polymer substrate by irradiation through a mask. The dimension of the film is 1 cm².

the number of silver ions in the feeding solution is not the limiting factor, we may explain this saturation by first considering the absorption of light by the silver particles within the film, which competes with the absorption from TiO₂ particles, leading to a self-limitation of the metal deposition. In this case, one expects a gradient of silver particles in the film thickness, which can indeed be observed in the TEM picture of a cross-section at least for short irradiation times (figure 4(b)). An iterative calculation of the silver distribution in the film as a function of the irradiation time was achieved by dividing the film thickness into multiple layers (details of the calculation are provided in the supplementary information, available at stacks.iop.org/Nano/23/505206/mmedia). The silver reduction yield was assumed to be constant and equal to 51% and its extinction coefficient at the irradiation wavelength was taken as $\alpha_{Ag} = 1/41 \text{ nm}^{-1}$. As shown in figure 5(a), the result consists of a significant decrease of the reduction rate corresponding to a competitive silver absorption. Nevertheless, the effect does not appear to be limiting enough to account for the clear saturation observed in the experimental results.

An additional effect has thus to be considered, associated with the maximum silver content in the film. In the initial calculation, this value was fixed to 100% volume fraction, which is evidently not possible considering that a part of the volume is occupied by TiO₂ and SiO₂. When a maximum silver loading of 16% is introduced, the iterative calculation matches well the kinetics data curve, showing that both effects of absorption and maximum loading should be taken into account (figure 5(a)). An interesting result of the calculation concerns the silver distribution within the film thickness (figure 5(b)). For limited irradiation times, the filling of the film with silver is progressive, starting from the interface close to the solution. The expected gradient of silver loading is consistent with the TEM profile as shown in figure 4(b) and, as discussed above, directly results from the competitive absorption effect of deposited silver. For higher irradiation times, we observe a progressive saturation within the whole film thickness (at the fixed value of 16%), leading to a final homogeneous distribution of silver loading throughout the film thickness. To confirm this result, we performed an experiment with a film having half the thickness of our standard samples (225 nm instead of 450 nm). The final silver

loading was still found to be 16%, which would not have been the case if a significant gradient of silver loading was present at the saturation.

Concerning the maximum value of silver loading, its value was found to be typically 16–18% in standard samples (depending on the total irradiation time). Previous characterizations of the initial films have shown that the maximum porosity available for silver growth, corresponding to the total porosity of the silica binder between the TiO₂ particles, is estimated to 26% in volume [17]. No distinction should be made between mesopores and micropores, considering that the size of the silver particles is much larger than the size of the mesopores (5 nm). We conclude that the growth of the silver particles near the TiO₂ particles fills part of the available porosity and this requires some densification of the porous silica network. The difference between the saturated silver loading (18%) and the initial available porosity (26%) can be explained considering that the silica densification could hardly be complete. Another point is that no significant evolution of the film thickness was detected after the silver loading. We can conclude that the saturation of the silver loading results from a mechanical effect associated with the limited possible plastic deformation of the SiO₂ binder. This also explains the efficiency of the mesoporous silica top layer buffer deposited at the surface of the active coating to confine the silver growth in the film.

3.4. Physical properties of the films: conductivity

A straightforward study of highly silver loaded films is to measure their electrical conductivity. Figure 6 shows the evolution of the conductivity measured on 24 different samples of CG-TiO₂ and S-TiO₂ loaded films obtained after different irradiation times. The results are plotted against the silver volume fraction.

After about 6 min of irradiation under standard conditions, a clear transition is observed in the conductivity curve corresponding to about 9–10% of silver loading. No significant differences are observed between CG-TiO₂ and S-TiO₂ loaded films, which is attributed to the fact that a high silver loading has erased the initial difference of silver distribution within the films observed at short irradiation times (figure 3). The well defined transition in

conductivity reveals a percolation threshold of the silver network leading to a conductivity of about 40 S cm^{-1} . This value is consistent with the one reported in previous works [16] or assembly of colloidal silver nanoparticles [25]. It is much lower than the conductivity of bulk silver ($6 \times 10^5 \text{ S cm}^{-1}$ [26]) due to the high granularity and high dispersion state of the metal. Investigation of the evolution of the resistance as a function of temperature confirms a metallic conduction behavior for temperatures down to about 20 K (figure 6 supplementary information, available at stacks.iop.org/Nano/23/505206/mmedia). Below this temperature, a positive to negative transition of the temperature coefficient of resistance (TCR) is noted, as already observed in an assembly of nanoparticles and explained as a result of carrier localization [25, 27].

An interesting application of the process comes from the possibility to perform the film deposition and photo-reduction of silver at low temperature, thus allowing silver patterning on polymer substrates. As compared to other systems [16, 27–29], we here take advantage of the use of preformed colloidal TiO_2 nanoparticles that exhibit a good crystallinity and therefore an excellent photocatalytic activity without the requirement of any thermal post-treatment of crystallization. In these experiments, no calcination was performed after the film deposition and irradiation was achieved in the presence of the copolymer template. In this case, we found no significant difference as compared to calcined films in terms of silver loading and conductivity. Figure 6(b) shows an example of silver patterns obtained on a polymer substrate after irradiation through a patterned mask. This method provides a simple way for lithographic deposition of electrical contacts. Although the conductivity should be improved (e.g. by increasing the initial porosity of the films) and stability issues should be addressed, this opens the way to applications in organic electronics, similarly to other methods such as electroless deposition or ink-jet printing of conductive electrodes [30, 31].

3.5. Physical properties of the films: photochromism

Numerous investigations of Tatsuma and co-workers [10–13] have evidenced the interesting photochromic properties of the Ag/TiO_2 hybrid materials. This phenomenon is shown by irradiating a sample with light at a wavelength higher than typically 450 nm, corresponding to the shape sensitive region in the spectra of silver particles. Selective illumination reduces the extinction at the wavelength of irradiation and apparently the resulting spectral hole turns the color of the illuminated region into that of the illuminating light. Indeed, this change of color is due to the fact that, at the irradiation wavelength, the photochromic sample becomes less absorbing for say the red light, which is therefore more reflected when illuminating the sample with a white lamp. This effect is also enforced by the fact that the change induced by the selective laser excitation is not only in the spectral domain, but also in the spatial domain, and the contrast between the irradiated area compared to the nonirradiated surroundings is also increased. We performed these experiments on silver

loaded films in air through irradiation with laser beams at 405 nm (blue, $P = 190 \text{ mW cm}^{-2}$), 532 nm (green, $P = 260 \text{ mW cm}^{-2}$) and 633 nm (red, $P = 530 \text{ mW cm}^{-2}$) respectively. After only a few minutes of irradiation, the green and red irradiated spots clearly appear with a color that corresponds to that of the laser source, for the reason explained above.

The mechanism of this effect has been discussed in previous works [11, 12, 32]. Irradiation at the wavelength of absorption of silver leads to some back electron transfer from the metal to the semiconductor. This corresponds to a selective dissolution of the particles whose configuration corresponds to plasmonic absorption at the wavelength of irradiation. Figure 7 presents the evolution of the absorbance observed on our samples. In the three conditions of irradiation, there is a decrease of the plasmonic absorbance at the wavelength of irradiation, associated with an increase of the absorption at some other wavelengths. This shows that there is some photodissolution of the silver phase, which is further redistributed to some configurations (in term of shape or interparticle distance) whose plasmonic absorption is lower at the excitation wavelength. It is known that the contribution around 410 nm is common to almost all silver nanostructures considering small particles in interaction or with anisotropic shapes. This explains that photodissolution at 532 and 633 nm causes a redistribution into structures with an increase of the absorbance at 410 nm, while the dissolution process resulting from the excitation at 405 nm is much slower (about tenfold). Interestingly, we observe that, for samples irradiated at 532 and 633 nm, the spectral changes exhibit an isobestic point, at least in the case when a sufficient silver loading was present initially. This shows that, in our samples, the redeposition of silver after photodissolution is almost complete. In their recent paper, Tatsuma and Kazuma discuss the influence of humidity, that appears to be essential for the redeposition process [33]. In our case, no special attention was paid to this parameter, but it is well known that microporous sol–gel silica adsorbs water to a high extent. This may explain the high efficiency of the redeposition process in our case. Our attempt to correlate the spectral evolution with some changes in the silver distribution within the film by electron microscopy has been unsuccessful as yet due to the large distribution of plasmonic configurations in our films and the poor contrast in highly silver loaded films. Such investigation is under consideration on isolated TiO_2 particles.

4. Conclusion

The context of this work was the elaboration of metal/dielectric thin films through a photocatalytic process of photo-reduction starting from preformed TiO_2 nanoparticles dispersed within a mesoporous silica binder. Silver reduction is achieved by simple irradiation with a UV lamp of the $\text{TiO}_2/\text{SiO}_2$ film immersed in a solution of silver ions. This leads to the appearance of a color ranging from yellow to dark brown, which is characteristic of the silver nanoparticulate phase. The investigation of the kinetics of the silver loading shows a quantum yield of 51%, a high value explained by

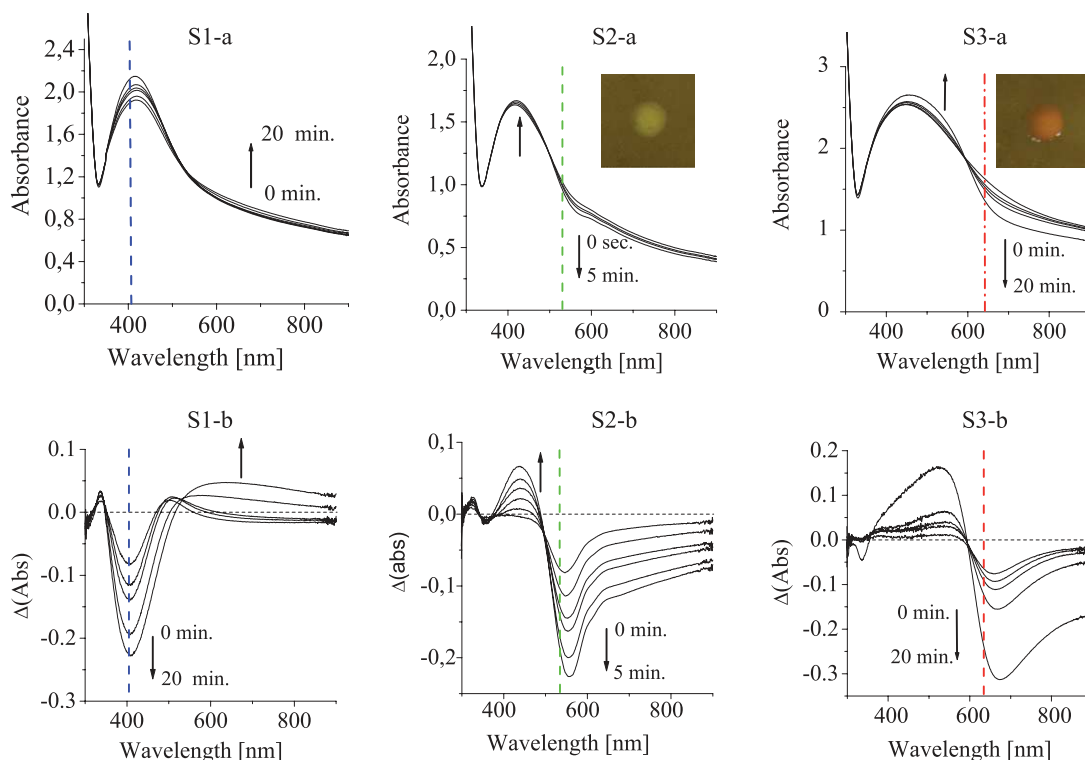


Figure 7. Absorption spectra (a) and absorbance change (b) of silver loaded samples (S1, 8.2 vol.%; S2, 7 vol.%; S3, 11 vol.%) irradiated with laser beams at 405 nm ($P = 190 \text{ mW cm}^{-2}$), 532 nm ($P = 260 \text{ mW cm}^{-2}$) and 633 nm ($P = 530 \text{ mW cm}^{-2}$) respectively.

the excellent crystallinity of the TiO_2 particles and the good accessibility of the silver ions to their surface. As a function of time, the silver profile develops with a gradient starting from the interface close to the solution. A maximum silver loading of 18% in volume is found. This value is shown to result from the available porosity of the silica binder and its limited plastic deformation due to the silica densification. When saturated, films are homogeneously filled throughout their thickness and exhibit metallic conduction properties with a conductivity of 40 S cm^{-1} . Irradiation through a mask on a polymer substrate permits the elaboration of contact patterns by a low-temperature process, which could find some interest for organic electronics. Finally, the photochromic properties of these films are characterized using irradiation of a silver loaded film at different wavelengths. This significantly changes the plasmonic absorption spectra, resulting in a local redistribution of the silver phase with a high efficiency. Such a method could be successfully applied to the engineering of the film properties, especially concerning plasmonics.

Acknowledgments

The authors wish to thank Kes van der Beek for the temperature dependent conductivity measurements and Jacques Peretti for his help in the modeling of the kinetics of silver loading. The Cristal Global Company is acknowledged for kindly providing samples of Cristal ACTiV™ S5-300 A TiO_2 dispersions.

References

- [1] Chen X and Mao S S 2007 *Chem. Rev.* **107** 2891
- [2] Fujishima A, Rao T N and Tryk D 2000 *J. Photochem. Photobiol. C* **1** 1
- [3] Huang M, Tso E and Datye A K 1996 *Environ. Sci. Tech.* **30** 3084
- [4] Jonker H, Kippel C J, Hutman H J, Janssen J G F and van Beek L K H 1969 *Photogr. Sci. Eng.* **13** 1
- [5] Pacholski C, Kornowski A and Weller H 2004 *Angew. Chem. Int. Edn Engl.* **43** 4774
- [6] Costi R, Saunders A E, Elmalem E, Salant A and Banin U 2008 *Nano Lett.* **8** 637
- [7] Carbone L, Jakab A, Khalavka Y and Sönnichsen C 2009 *Nano Lett.* **9** 3710
- [8] Costi R, Saunders A E and Banin U 2010 *Angew. Chem. Int. Edn Engl.* **49** 4878
- [9] Stathatos E, Lianos P, Falaras P and Siokou A 2000 *Langmuir* **16** 2398
- [10] Ohko Y, Tatsuma T, Fujii T, Naoi K, Niwa C, Kubota Y and Fujishima A 2003 *Nature Mater.* **2** 29
- [11] Matsubara K and Tatsuma T 2007 *Adv. Mater.* **19** 2802
- [12] Matsubara K, Kelly K L, Sakai N and Tatsuma T 2009 *J. Mater. Chem.* **19** 5526
- [13] Kawahara K, Suzuki K, Ohkowab Y and Tatsuma T 2005 *Phys. Chem. Chem. Phys.* **7** 3851
- [14] Naoi K, Ohko Y and Tatsuma T 2005 *Chem. Commun.* **1288**
- [15] Kelly K L and Yamashita K 2006 *J. Phys. Chem. B* **110** 7743
- [16] Martinez E D, Bellino M G and Soler-Illia G J A A 2009 *ACS Appl. Mater. Interface* **1** 746
- [17] Allain E, Besson S, Durand C, Moreau M, Gacoin T and Boilot J-P 2007 *Adv. Funct. Mater.* **17** 549
- [18] Gohin M, Allain E, Chemin N, Maurin I, Gacoin T and Boilot J-P 2010 *J. Photochem. Photobiol. A* **216** 142

- [19] Serpone N, Lawless D and Khairutdinov R 1995 *J. Phys. Chem.* **99** 16646
- [20] Liz-Marzan L M 2006 *Langmuir* **22** 32
- [21] Sahyun M R V and Serpone N 1997 *Langmuir* **13** 5081
- [22] Jakob M, Levanon H and Kamat P V 2003 *Nano Lett.* **3** 353
- [23] Besson S, Gacoin T, Ricolleau C and Boilot J-P 2003 *Chem. Commun.* 360
- [24] *Handbook of Optical Constants of Solids* 1985, ed E D Palik (New York: Academic)
- [25] Zabet-Khosousi A and Dhirani A-A 2008 *Chem. Rev.* **108** 4072
- [26] Weast R C and Shelby S M 1967–1968 *Handbook of Chemistry and Physics* 48th edn (Boca Raton, FL: CRC Press) p F-132
- [27] Quinn A J and Redmond G 2005 *Prog. Solid State Chem.* **33** 263
- [28] Crespo-Monteiro N, Destouches N, Bois L, Chassagneux F, Reynaud S and Fournel T 2010 *Adv. Mater.* **22** 3166
- [29] Martinez E D, Granja L, Bellino M G and Soler-Illia G 2010 *Phys. Chem. Chem. Phys.* **12** 14445
- [30] Li Y, Wu Y and Ong B S 2005 *J. Am. Chem. Soc.* **127** 3266
- [31] Polavarapu L, Manga K-K, Cao H-D, Loh K-P and Xu Q-H 2011 *Chem. Mater.* **23** 3273
- [32] Dahmen C, Sprafke A N, Dieker H, Wuttig M and von Plessen G 2006 *Appl. Phys. Lett.* **88** 11923
- [33] Kazuma E and Tatsuma T 2012 *Chem. Comm.* **48** 1733

Supporting Information

1. S-TiO₂ colloidal synthesis.

S-TiO₂ nanoparticles were prepared through a process adapted from Serpone et al. [35]. In a typical experiment, 135 mL of H₂O were added slowly into 3.5 mL of TiCl₄ under nitrogen atmosphere. The mixture was then left under stirring for 2 hours. Ethylene glycol was then added with an equal volume as the suspension and the mixture was heated for 8 h at 80°C to allow the crystallization of the anatase phase. The colloidal particles were recovered by centrifugation after addition of acetone. They were washed several times with water and finally dispersed in water acidified with HNO₃ at pH 1.25. The suspension has a TiO₂ content of 80g.L⁻¹ and the particles size as determined by dynamic light scattering measurement is 7 nm.

2. Experimental setup for the silver reduction experiment

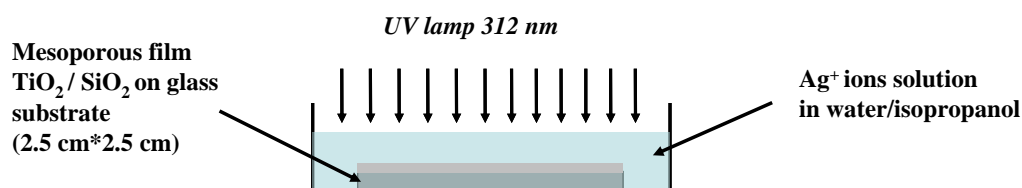


Figure 1 SI: Scheme of the experimental setup used for the photocatalytic photoreduction experiment. Note that for long irradiation time, a quartz cover plate is put on top of the beaker to avoid significant evaporation of the solvents.

3. Electron microscopy characterization of the effect of a porous silica top layer buffer.

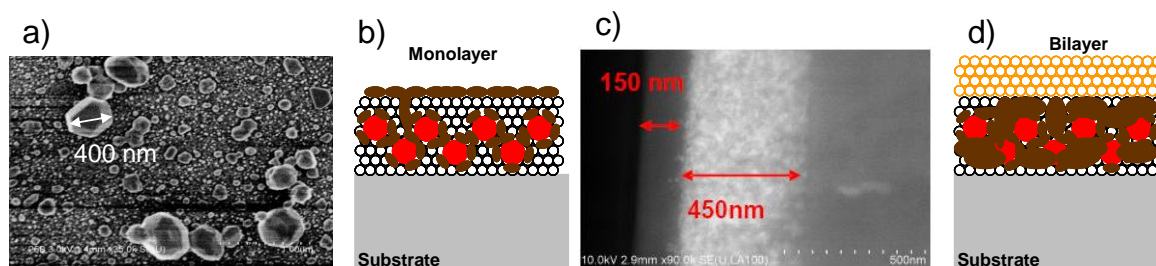


Figure 2 SI: Typical SEM image (top view) of a film without a porous silica top layer buffer, evidencing the formation of large silver crystals at the interface with the solution (a). Schematic representation of the mechanism responsible for the formation of these large crystals (b). TEM view (cross section) of a film saturated with silver showing the effect of the buffer layer on the homogeneity of the silver distribution (c). Schematic representation of the film (d).

4. Correlation between the silver volume fraction and the absorbance of the films at 320, 410 and 1000 nm.

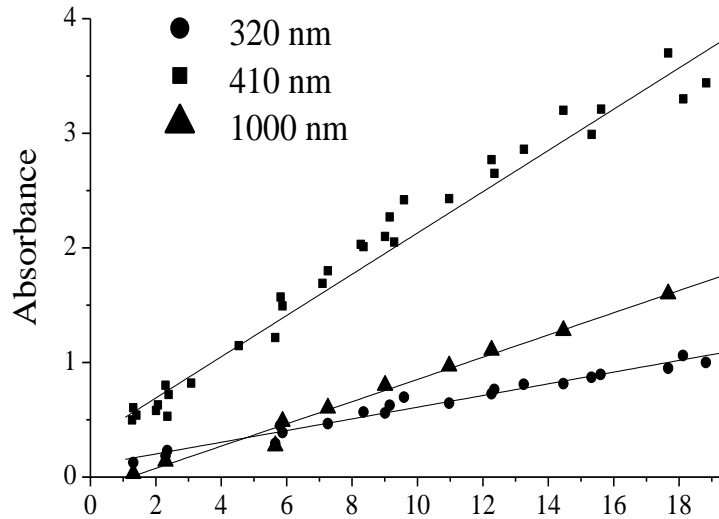


Figure 3 SI: Plot of the evolution of the maximum absorbance of the films (Ti/Si = 1) at 320, 410 and 1000 nm as a function of the silver loading measured by chemical analysis.

5. Spectra of the UV lamp and absorbance of the TiO₂ in the film.

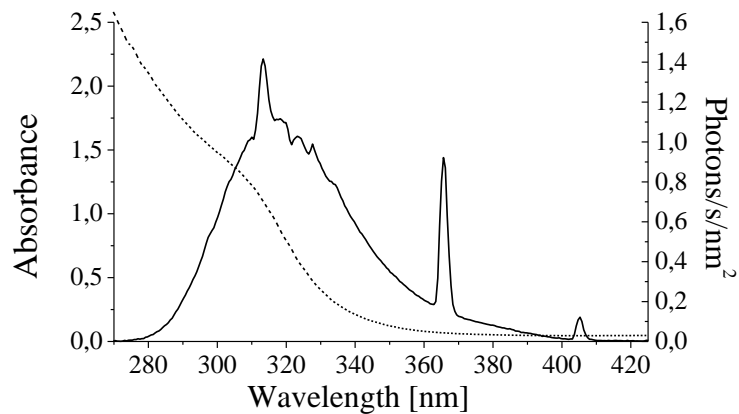


Figure 4 SI: Plot of the absorbance of the TiO₂ in the film (dotted curve) and emission spectrum of the 3.5 mW.cm⁻² UV lamp (plain curve).

6. Iterative calculation of silver reduction kinetic and profile in the film thickness, taking into account the competitive absorption from silver and TiO₂.

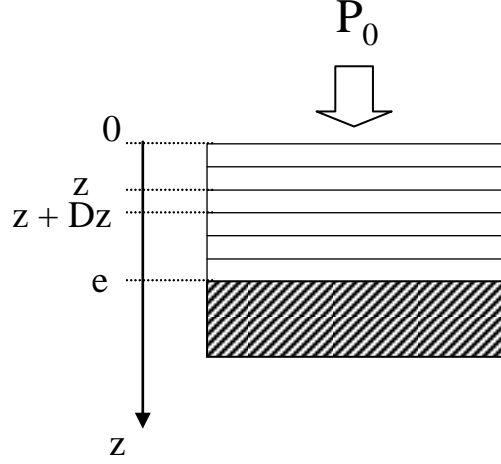


Figure 5 SI: Schematic representation of the active layer divided into several sublayers with thickness Δz for the iterative calculation.

We consider the active thin film with a thickness e as a stack of layers with a thickness Δz . The layer lying between z and $z+\Delta z$ will be called “layer z ”. P_0 is the incident light power (expressed in photons. $s^{-1}.cm^{-2}$). $P(z)$ is the power of excitation incoming in the z layer. $\rho_{Ag}(z)$ is the silver volume fraction in the layer z , supposed to be constant in the thickness of this layer. The number of atoms of silver formed per cm^2 between a time t and $t+\Delta t$ in the layer z is equal to the number of photons

absorbed by the TiO₂ in this layer. $N_{Ag}(z, t + \Delta t) = N_{Ag}(z, t) + \eta.P(z).(1 - 10^{-A_{TiO_2} \cdot \frac{\Delta z}{e}}).\Delta t$ [Eq. 1]

With A_{TiO_2} the overall absorbance of TiO₂ in the film and η the silver quantum yield of reduction determined as discussed in the main text and assumed to be constant with time.

The corresponding variation of silver volume fraction between t and $t+\Delta t$ in the layer z is then :

$$\rho_{Ag}(z, t + \Delta t) = \rho_{Ag}(z, t) + \eta.P(z) \cdot \frac{V_{Ag}}{N_A \cdot \Delta z} (1 - 10^{-A_{TiO_2} \cdot \frac{\Delta z}{e}}) \quad [Eq. 2]$$

Now, the power of excitation which exit from the layer z is derived both from the absorbance of the TiO₂ and the absorbance from the silver in the z layer :

$$P(z + \Delta z, t) = P(z, t) \cdot (1 - 10^{-A_{TiO_2} \cdot \frac{\Delta z}{e}} \cdot 10^{-\frac{\alpha_{Ag} \cdot \rho_{Ag}(z, t) \cdot \Delta z}{\ln(10)}}) \quad [Eq. 3]$$

Iterative calculation was performed using Mathematica® software. The values of absorbance from both silver and TiO₂ were considered at 312 nm, after considering that the global emission from the lamp (and thus integrating the above equations over its emission spectrum) does not change significantly our results. Times steps were normalized to fit the experimental kinetic experiments.

7. Resistance vs temperature curve for a film.

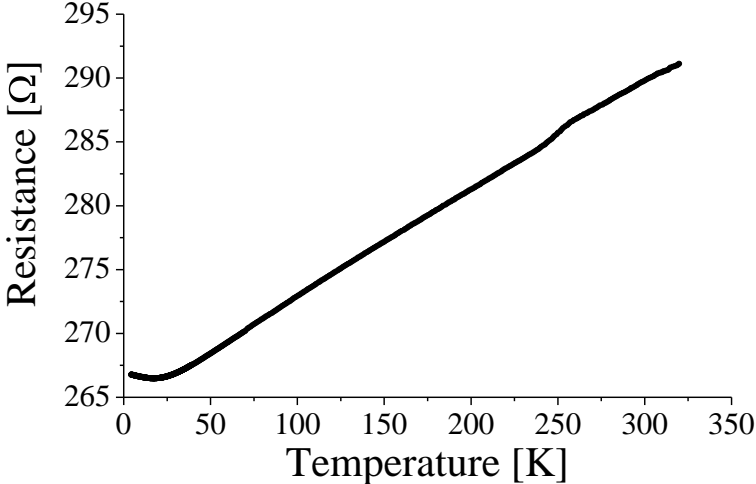


Figure 6 SI: Plot of the evolution of the resistance between two silver paint contacts on a conductive film as a function of the temperature, evidencing for the metallic conduction mechanism above about 20K.